Thermodynamic Model for the Stabilization of Trigonal Thiolato Mercury(II) in Designed Three-Stranded Coiled Coils[†]

Brian T. Farrer, Nzingha P. Harris, Kristen E. Balchus, and Vincent L. Pecoraro*

Department of Chemistry, The University of Michigan, Ann Arbor, Michigan 48109-1055

Received August 6, 2001; Revised Manuscript Received October 5, 2001

ABSTRACT: A thermodynamic model is presented that describes the binding of Hg(II) to de novo designed peptides, Tri L9C and Baby L9C, which were derived from the Tri family. The Tri peptides are based on the parent sequence Ac-NH-G(LKALEEK)$_x$G-CONH$_2$ and are known to form two-stranded coiled coils at low pH (pH <4) and three-stranded coiled coils at high pH (pH >7). Tri L9C ($x = 4$) contains a four heptad repeat sequence with cysteine in position 9 and leucines in the other a and d positions; Baby L9C ($x = 3$), which also has a cysteine in position 9 but is one heptad shorter than Tri L9C, was designed to form less stable helical coiled coils in solution. The free energies of coiled coil formation for Tri, Tri L9C, Baby Tri, and Baby L9C at pH 2.5 and 8.5 were determined by guanidinium denaturation titrations; Tri L9C was observed to be highly helical in the absence of denaturant at pH 8.5 while Baby L9C contained <20% helical content at pH 8.5, indicating a weakly associated or unassociated coiled coil. Size-exclusion chromatography (SEC) verified that Baby L9C was a monomer at pH 8.5. The helicity of Baby L9C was induced by addition of $HgCl_2$. The subsequent formation of a trigonal thiolato Hg(II) in the interior of a three-stranded coiled coil was verified by the presence of a characteristic HgS_3 UV band at 248 nm. Titrations of Tri L9C and Baby L9C into solutions of $HgCl_2$ at pH values between 7 and 9 were performed to extract binding constants. Global fits to the data employed a mechanism that involved initial binding of mercury to the peptides forming a two-stranded coiled coil with linear thiolato Hg(II) at [peptide]/[Hg] <2, followed by addition of a more weakly associated third helix to generate a three-stranded coiled coil. This mechanism would require the deprotonation of the third cysteine thiol to generate the trigonal thiolato Hg(II) at pH >7.5 [the pK_a of the cysteine thiol in the presence of Hg(II)]. Support for this mechanism was given by the observation of a three-stranded coiled coil by SEC in a solution of Tri L9C at pH 7.0.

The field of peptide and protein design offers a powerful approach to understanding of protein structure and folding dynamics (*1*−*4*). In particular, the past decade has seen investigation into metalloprotein structure using design techniques (*1*, *5*−*7*). These efforts have been directed toward determining the fundamental forces involved in metalloprotein folding, structure, and function. A simplified view of the forces influencing overall metalloprotein structure suggests involvement of two primary factors: (a) the driving force for metal coordination geometry with a particular ligand donor set and (b) the driving force directing the fold of the polypeptide chain. This simplification allows metalloprotein structure to be defined in two ways. First is the case where metal coordination preferences dominate overall folding energy to determine the metalloprotein structure. A good biological example is found in the zinc finger motif (*8*). Prior to metal binding, the oligopeptide chain of a zinc finger is generally unstructured. Addition of zinc drives the formation of the characteristic $\beta_2\alpha$ fold by the formation of a tetrahedral Cys$_x$His$_{4-x}$ zinc center. In the second case, polypeptide backbone folding energetics dominate the overall fold of the metalloprotein, forcing a desired coordination environment around a metal. One of the best biological examples of this case is found in the blue copper protein azurin. The polypeptide chain of azurin in the absence of copper closely resembles the fold of the protein chain with copper bound. This rigidity is used to stabilize the copper(I) form of the enzyme with respect to the copper(II) form. Consequently, the copper is endowed with desired electrochemical properties that allow it to carry out its function in living systems (*9*).

In efforts to understand natural proteins, these two extremes have been utilized by protein designers to create novel protein constructs and to create new enzymatic systems. For example, the driving force for Ru(trisbipyridine)$^{2+}$ formation has been used in the stabilization of three-stranded coiled coils (*5*, *10*, *11*). These ruthenium-modified synthetic metallopeptides have been used to study electron transfer through a polypeptide backbone (*12*). Other peptides containing polypyridyl complexes of ruthenium allowed study of electron transfer across α-helices (*13*, *14*). Three-stranded coiled coils were also assembled by coordination of histidines to Co(II), Ni(II), Cu(II), and Zn(II) (*15*). As an example of the opposite case, where the polypeptide fold determines the overall structure of the metallopolypeptide, our laboratory has used very stable three-stranded coiled coil

[†] This work was supported by the NIEHS, NRSA Grant 1F32 ES05888-01.

* To whom correspondence should be addressed. E-mail: vlpec@umich.edu. Phone: 734-763-1519. Fax: 734-936-7628.

10.1021/bi015649a CCC: $20.00
Published on Web 11/07/2001

Table 1: Amino Acid Sequences of Peptides

Peptide	Sequence
position	*g abcdefg abcdefg abcdefg abcdefg a*
Tri	Ac-G LKALEEK LKALEEK LKALEEK LKALEEK G-NH_2
Tri L9C	Ac-G LKALEEK **C**KALEEK LKALEEK LKALEEK G-NH_2
Tri L12C	Ac-G LKALEEK LKA**C**EEK LKALEEK LKALEEK G-NH_2
Tri L16C	Ac-G LKALEEK LKALEEK **C**KALEEK LKALEEK G-NH_2
Baby Tri	Ac-G LKALEEK LKALEEK LKALEEK G-NH_2
Baby L9C	Ac-G LKALEEK **C**KALEEK LKALEEK G-NH_2

peptides, Tri[1] L9C and Tri L16C (Table 1), in aqueous solutions to form trigonal thiolato ligation environments around Hg(II), a metal which in aqueous solution at micromolar concentrations prefers linear coordination by simple thiolates (*16*, *17*).

Linear Thiolato Hg(II) Trigonal Thiolato Hg(II)

Another approach to metalloprotein design is the use of algorithms that determine the optimal location for incorporating a metal binding site onto a protein (*6*, *18*−*20*). Thus, metal binding sites have been inserted via mutagenesis into proteins that do not have intrinsic metal centers (e.g., thioredoxin). Many of the metal cofactors routinely used by natural systems have been successfully incorporated. Also, a zinc sensor was designed from a maltose receptor by insertion of a Zn coordination site between two domains of the receptor. To accommodate a dominant zinc coordination preference, the protein structure is perturbed; this change in overall structure was monitored by a fluorescent tag attached to a protein signaling the presence of zinc (*21*).

Many natural metalloproteins incorporate a cooperative protein fold, in which the final protein structure upon metal incorporation contains neither the preferred metal coordination environment nor the desired polypeptide backbone structure as determined by the apoprotein. One well-documented example is cytochrome *c* (*22*). The folding of cytochrome *c* occurs in two experimentally distinguishable kinetic steps. The first of these steps involves collapse of the protein structure around a heme cofactor that produces an intermediate containing a favorable iron coordination environment. The second step is rearrangement of the polypeptide chain driven by the conformation preferences of the peptide accompanied by ligand exchange on the metal so that the resulting coordination environment is a consequence of both the protein folding preference and the metal coordination preference. Metalloprotein design has recently begun to focus on this "gray" area of cooperative binding; iterative design strategies have been employed in the stabilization of an Fe_4S_4 cluster (*23*, *24*), a method requiring sequential redesign of the protein sequence based on the stability of the ultimate metalloprotein construct. Also, Li et al. reported a peptide, IZ-AC, that is unstructured prior to addition of metal and binds Hg(II) with trigonal thiolato coordination (*25*).

As mentioned above, our group has studied de novo designed α-helical coiled coils containing thiolate ligands based on the sequence of Tri (Table 1) (*16*, *17*), a 30 amino acid peptide of regular heptad repeats with leucines in the a and d positions. Tri is known to fold into a well-defined, stable three-stranded coiled coil at neutral pH. At lower pH (pH <4) the peptide was observed to form a very stable two-stranded coiled coil with a well-defined transition (pH 4−7) between the two- and three-stranded coiled coils. Substitution of one of the leucines for cysteine results in a peptide, Tri L9C, containing a soft-metal binding site. This peptide has been shown to bind Hg(II) at pH >7 with trigonal thiolate ligation similar to that found in the protein MerR (*26*).

The present report introduces a novel peptide, Baby L9C, which is shorter than Tri L9C by one heptad. Baby L9C did not form a well-defined three-stranded coiled coil in solution prior to addition of Hg(II). It does, however, bind Hg(II) with trigonal thiolato coordination with concurrent formation of an α-helical coiled coil. Thus, the Hg:Baby L9C system displays a final peptide structure that is determined neither by the coordination preference of the metal nor by the rigid backbone structure of the peptide coiled coil. A robust thermodynamic model is also presented that quantitatively describes not only the formation of the Hg(II) three-stranded coiled coil for both Tri L9C and Baby L9C but also the pH dependences of Hg(II) binding to both peptides. This model proposes that trigonal thiolato Hg(II) formation is dependent not only on the formation of the three-stranded coiled coil but also on the deprotonation of a cysteine thiol within a three-stranded coiled coil. Evidence for the formation of a linear two-coordinate Hg(II) encapsulated in a three-stranded coiled coil is presented to support this model.

EXPERIMENTAL PROCEDURES

Peptide Synthesis and Purification. All peptides were synthesized on a Milligan Model 9050 Plus continuous-flow peptide synthesizer using Fmoc-protected amino acids (Novabiochem) with OPfp/HOBt activation. The N-termini of the peptides were acetylated prior to cleavage using acetic anhydride/pyridine in dimethylformamide. Peptides were synthesized on a Rink amide resin (~0.5 mmol/g substitution, NovaBiochem), yielding the C-terminal amide upon cleavage with 95% trifluoroacetic acid. Thioanisole, anisole, and ethanedithiol were used as scavengers in the cleavage reactions. Peptides were purified by preparative reversed-phase C18 HPLC using a flow rate of 10 mL/min and a linear gradient of 0.1% TFA in water to 0.1% TFA in 9:1 CH_3-CN:H_2O over 50 min. Peptides were identified with MALDI and electrospray mass spectrometry (Protein and Carboydrate Structure Facility, University of Michigan). Concentrations of peptide stock solutions were determined using a number of methods: circular dichroism optical activity in 50% trifluoroethanol with comparison to those observed by Su et al. (*27*), addition of 5,5′-dithiobis(2-nitrobenzoic acid) with subsequent monitoring at 410 nm to determine cysteine concentration (Ellman's test), and/or amino acid analysis

[1] Abbreviations: Tri, peptide with the sequence CH_3CO-G(LKALEEK)$_4$G-NH_2; Baby Tri, peptide with the sequence CH_3CO-G(LKALEEK)$_3$G-NH_2; SEC, size-exclusion chromatography; GuHCl, guanidinium chloride; SimAD, simultaneous aggregation−deprotonation; StepAD, stepwise aggregation−deprotonation; Ac, acetyl group (CH_3CO−).

(Protein and Carboydrate Structure Facility, University of Michigan).

Guanidinium Denaturation Titrations. GuHCl titrations were performed by a Microlab 500 series automatic titrator (Hamilton Co.) controlled by AVIV-supplied software. The titrations were carried out by mixing separate solutions (0 and 7.5 M) of GuHCl; the concentration of the guanidinium was obtained from refractive index measurements (*28*). Each solution contained 50 mM phosphate and 3−7 μM peptide. The pH of both solutions was adjusted to the desired value using an Accumet gel-filled pencil-thin Ag/AgCl single-junction electrode attached to an Orion Research digital pH/millivolt meter 611. Titrations were performed at 25 ± 1 °C in a 1 mm path-length rectangular quartz cell. For every point, the sample was stirred for 60 s, and data were collected for 2 s and averaged to obtain the signal. The mean residue ellipticity was calculated using $[\theta]_{222} = \theta_{obs}/(10lcn)$, where θ_{obs} is the observed ellipticity in millidegrees, l is the path length of the cell in centimeters, c is the peptide concentration in moles per liter, and n is the number of residues per peptide.

Analyses of the guanidinium chloride titrations were performed to extract formation constants of the peptide coiled coils by a previously described combined numerical and nonlinear least-squares fitting to the data (*17*, *29*, *30*). These calculations were performed using MatLab v5.2.1 (The Mathworks, Inc.). The initial estimates for the fits were obtained by evaluation of the titration curves as described by Pace and Sholtz (*28*).

Hg(II) Titrations. Hg(II) titrations were monitored from 200 to 320 nm on a Perkin-Elmer Lambda 9 UV/vis/NIR spectrophotometer. All solutions were purged with argon and were blanketed with N_2 during titrations. Peptides were added from stock solutions (~1.5 mM) in 2−4 μL aliquots into a 2.5 mL solution of 5−20 μL $HgCl_2$ in 10 mM phosphate buffer. For each aliquot, an equivalent amount of peptide was added to the background solution so the difference spectra contained only the absorbances attributable to the presence of $HgCl_2$ and peptide conformational changes. After each aliquot, the solutions were allowed to equilibrate for 1 min in the case of Baby L9C and 10−20 min in the case of Tri L9C.

These titrations were analyzed using the global analysis program SPECFIT (Spectrum Software Associates), which couples linear least-squares fitting and factor analysis by singular value decomposition. The thermodynamic model used to fit the data is given in eq 1 and included formation

$$m\mathrm{Hg(II)} + l\mathrm{L}^- + h\mathrm{H}^+ \rightleftharpoons [\mathrm{Hg}_m(\mathrm{LH})_h(\mathrm{L})_{l-h}]^{+(2m+h-l)} \quad (1)$$

constants, β_{mlh}, where m, l, and h are the stoichiometries of metal, peptide, and cysteine protons within the complex, respectively. Specifically, the model contained formation constants for protonated peptide (β_{011}), three-stranded coiled coil (β_{033}), two-stranded coiled coil with coordinated Hg^{2+} (β_{120}), three-stranded coiled coil with linearly coordinated Hg^{2+} (β_{131}), and three-stranded coiled coil with trigonally coordinated Hg^{2+} (β_{130}). In this representation the formation constants of Hg^{2+} (β_{100}), H^+ (β_{001}), and deprotonated peptide (β_{010}) are set to 1:

$$\mathrm{L}^- + \mathrm{H}^+ \overset{\beta_{011}}{\rightleftharpoons} \mathrm{LH} \qquad \beta_{011} = \frac{[\mathrm{LH}]}{[\mathrm{L}^-][\mathrm{H}^+]} \quad (2)$$

$$3\mathrm{L}^- + 3\mathrm{H}^+ \overset{\beta_{033}}{\rightleftharpoons} (\mathrm{LH})_3 \qquad \beta_{033} = \frac{[(\mathrm{LH})_3]}{[\mathrm{L}^-]^3[\mathrm{H}^+]^3} \quad (3)$$

$$\mathrm{Hg(II)} + 2\mathrm{L}^- \overset{\beta_{120}}{\rightleftharpoons} \mathrm{Hg(L)}_2 \qquad \beta_{120} = \frac{[\mathrm{HgL}_2]}{[\mathrm{Hg(II)}][\mathrm{L}^-]^2} \quad (4)$$

$$\mathrm{Hg(II)} + 3\mathrm{L}^- \overset{\beta_{130}}{\rightleftharpoons} [\mathrm{HgL}_3]^- \qquad \beta_{130} = \frac{[(\mathrm{HgL}_3)^-]}{[\mathrm{Hg(II)}][\mathrm{L}^-]^3} \quad (5)$$

$$\mathrm{Hg(II)} + 3\mathrm{L}^- + \mathrm{H}^+ \overset{\beta_{131}}{\rightleftharpoons} \mathrm{Hg(LH)(L)}_2 \qquad \beta_{131} = \frac{[\mathrm{Hg(LH)L}_2]}{[\mathrm{Hg(II)}][\mathrm{L}^-]^3[\mathrm{H}^+]} \quad (6)$$

β_{130} and β_{131} were variables in the fits. β_{011} was defined as $10^{8.5}$ M^{-1} corresponding to the pK_a of free cysteine in aqueous solution, $\beta_{120} = 10^{60}$ M^{-2} corresponds to the formation of linear mercury with simple thiolate ligands (*26*), and β_{033} corresponds to the formation constants of the three-stranded coiled coils determined by guanidinium denaturation titration data summarized in Table 2.

pH Titrations. pH titrations were monitored from 200 to 320 nm on a Perkin-Elmer Lambda 9 UV/vis/NIR spectrophotometer. All solutions were purged with Ar, and N_2 was bubbled through the solutions during titrations. Fifteen milliliter solutions of 50 μM peptide and 10 μM $HgCl_2$ were titrated from pH 3 to pH 9 by adding small aliquots of 1 mM to 1 M solutions of potassium hydroxide and monitoring the pH using an Accumet gel-filled pencil-thin Ag/AgCl single-junction electrode with an Orion Research digital pH/millivolt meter 611. Reverse titrations (pH 9 to pH 5) were performed by adding small aliquots of 1 mM to 1 M solutions of hydrochloric acid.

Size-Exclusion Chromatography. Size-exclusion chromotagraphy was carried out using a Pharmacia Superdex 75 column and a Pharmacia P-500 pump. As(III)-containing peptides were used as three-stranded coiled coil references (*31*); peptides resulting from cysteine oxidation were used along with peptide solutions containing 0.5 equiv of $HgCl_2$ as references for two-stranded coiled coils.

For the pH titrations of Tri L9C using SEC, samples contained 0.10 mM peptide and 0.033 mM $HgCl_2$ in a solution containing 150 mM KCl and 100 mM potassium phosphate buffered to the desired pH. Samples were run at 0.5 mL/min using a solution containing 150 mM KCl and 100 mM potassium phosphate buffered to the desired pH as an eluant; the chromatography for Baby L9C was carried out under similar conditions. The results of these experiments were evaluated by comparing the position of the sample peak relative to those of the reference peaks. Since retention time of the peptide varied with pH, the position of the specific peak was represented as a function of the reference peaks for the two- and three-stranded coiled coils:

$$\chi(\mathrm{sample}) = [\mathrm{RT(sample)} - \mathrm{RT(dimer)}]/[\mathrm{RT(trimer)} - \mathrm{RT(dimer)}]$$

RESULTS

Synthesis. Solid-phase peptide synthesis has been employed by our laboratory to obtain Tri, Tri L9C, and other singly substituted analogues of Tri (*16*, *17*); the same procedure was used for the preparation of Baby Tri and Baby

Table 2: Formation Constants for Two- and Three-Stranded Coiled Coils at pH 2.5 and 8.5, Respectively, As Determined by Fits to the Guanidinium Denaturation Data Given in Figure 1

peptide	n[a]	pH	$1/K_a$ (M or M^2)	$-\Delta G$ (kcal/mol)	m_g[b] (kcal/mol)
Tri[c]	2	2.5	1.3×10^{-15}	20.3 (10.2)	2.3
	3	8.5	5.9×10^{-18}	23.5 (7.8)	2.7
Baby Tri	2	2.5	3.1×10^{-9}	11.6 (5.8)	1.2
	3	8.5	2.7×10^{-11}	14.4 (4.8)	1.0
Tri L9C[c]	2	2.5	2.2×10^{-12}	15.9 (8.0)	1.8
	3	8.5	4.4×10^{-14}	18.2 (6.1)	1.9
Baby L9C	2	2.5	1.4×10^{-6}	8.0 (4.0)	1.0
	3	8.5	$\sim 10^{-8}$	~ 10 (~ 3)[d]	n/a

[a] n is the aggregation state for the coiled coil ($n = 2$ indicates a two-stranded coiled coil; $n = 3$ indicates a three-stranded coiled coil). [b] m_g quantifies the effect of guanidinium on the free energy of folding $\Delta G^\circ = \Delta G^\circ_{0M} + m_g$[GuHCl], where ΔG°_{0M} is the free energy of folding in the absence of guanidinium chloride. [c] The values for Tri at pH 2.5 and 8.5 as well as Tri L9C at pH 2.5 were taken from ref *16*. [d] The value for Baby L9C at pH 8.5 was estimated from the CD signal at [GuHCl] = 0 M.

L9C, which have seven fewer residues (one less heptad) than Tri and Tri L9C. Removal of one heptad in the Baby peptides deletes two complete turns of the α-helix. All of the peptides were synthesized on a modified Rink amide resin, resulting in the amidation of the C-terminus. The peptides were also acylated on the N-terminus at the end of the synthesis with acetic anhydride.

Guanidinium Denaturations. The stabilities of the resulting peptide coiled coils for each of the peptides were determined by monitoring the circular dichroism signal at 222 nm during the addition of guanidinium chloride. Previous work on the Tri series of peptides showed that the low-pH (pH <5) form of the coiled coil was more stable (per strand) than the high-pH form (pH >7) (*16*); the low- and high-pH forms were identified by analytical ultracentrifugation to be two- and three-stranded coiled coils, respectively. In this study, Baby Tri and Baby L9C showed the same pH dependence on stability (Figure 1). For Baby L9C, the CD signal at 0 M GuHCl is only −10 deg cm^2 $dmol^{-1}$.

The titrations at both low and high pH were analyzed using a combined numerical and nonlinear least-squares fitting procedure from which were obtained free energies of coiled-coil formation (*17*, *29*, *30*). The stability of Baby L9C was estimated from the fraction of α-helical content because it did not form a complete structure in pH 8.5 buffer at 0 M GuHCl. The data (Table 2) indicate that 4−5 kcal/mol and ∼3 kcal/mol per peptide were lost by removal of one heptad from the two- and three-stranded coiled coils, respectively. Destabilization by 3 kcal/mol was similar to what Su et al. have observed for three-stranded coiled coils with a leucine core (*27*). The data also showed that the effect of substituting a cysteine for a leucine on the stability of the peptide coiled coil was about 2 kcal/mol per peptide for either coiled-coil aggregate. Thus, simultaneously removing both a heptad from the parent peptide Tri and replacing a leucine with a cysteine should result in a peptide whose three-stranded coiled coil would be destabilized by ∼5−6 kcal/mol per peptide; such an aggregate at micromolar concentrations is predicted to be unstable at pH 8.5. This prediction is verified by Baby L9C.

UV−Visible Titrations. Both the linear thiolato Hg(II) complex, $Hg(SR)_2$, and the trigonal thiolato Hg(II) complex,

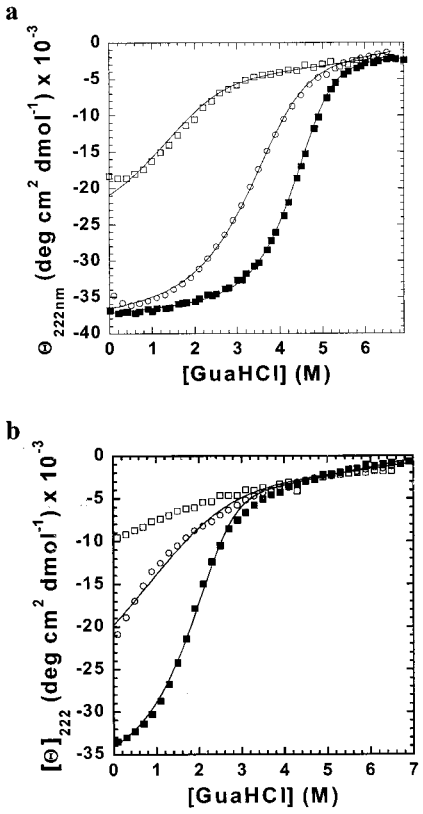

FIGURE 1: Guanidinium denaturation titrations and fits to the data for Baby (○), Baby L9C (□), and Tri L9C (■) at (a) pH 2.5 and (b) pH 8.5. Lines show fit to the data using a combined numerical and nonlinear least-squares fitting described previously (*17*, *29*, *30*).

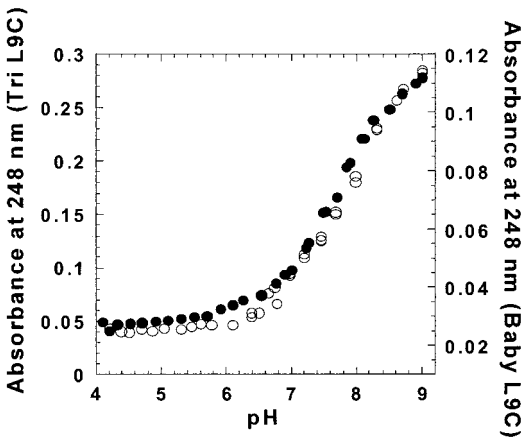

FIGURE 2: pH titration of a solution containing 30 μM peptide and 10 μM $HgCl_2$ for both Tri L9C (●) and Baby L9C (○). The titration is monitoring the formation of the trigonal thiolato Hg(II) complex by observing the maximum of the trigonal thiolato Hg(II) MLCT band at 248 nm. pK_a(apparent) is 7.8 ± 0.4 for Baby L9C and 7.6 ± 0.2 for Tri L9C.

$Hg(SR)_3^-$, have a ligand-to-metal charge transfer (LMCT) band in the UV (200−320 nm). $Hg(SR)_3^-$ has a characteristic lower energy absorbance at 248 nm distinguishable from the higher energy transition of $Hg(SR)_2$. Figure 2 shows a pH titration (pH 4−9) of a solution containing 30 μM peptide and 10 μM $HgCl_2$ monitoring at absorbance maximum for the $Hg(SR)_3^-$ LMCT band (248 nm); the apparent pK_a values of $Hg(SR)_3^-$ formation in both Tri L9C and Baby L9C were determined to be 7.6 ± 0.2 and 7.7 ± 0.2, respectively.

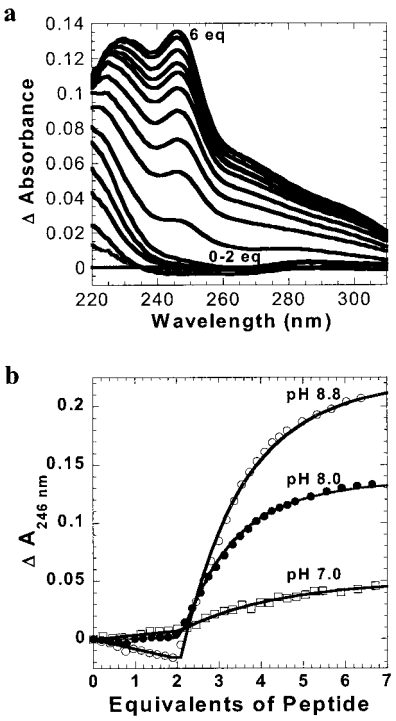

FIGURE 3: (a) Difference spectra in a sample titration of Baby L9C into a solution of 50 mM potassium phosphate (pH 8.0) containing 10 μM $HgCl_2$. The background solution for the titration is identical to the sample solution without $HgCl_2$. (b) Titrations and global fits to the data using the StepAD mechanism for Baby L9C addition to a solution of 10 μM $Hg^{II}Cl_2$ at pH 7.0, 8.0, and 8.8. Shown are traces from the data and fits at 246 nm.

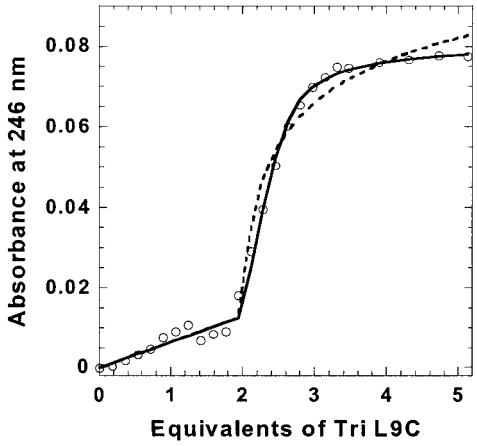

FIGURE 4: Titration of Tri L9C into a solution of 5 μM $Hg^{II}Cl_2$ at pH 7 showing two fits to the data. The SimAD model is shown as a dashed line, and the StepAD model is shown as a solid line.

A titration of Baby L9C into a solution of 10 μM Hg(II) at pH 8.8 was monitored between 220 and 320 nm (Figure 3a). As up to 2 equiv of peptide was added, the characteristic signal for $Hg(SR)_3^-$ was not observed. However, the $Hg(SR)_3^-$ signal developed immediately when more than 2 equiv of peptide was present. Titrations were performed at pH 7.0, 8.0, and 8.8 for both Tri L9C and Baby L9C. The set of titrations for Baby L9C is shown in Figure 3b. Three distinct observations can be made when the different pH titrations are compared. First, at no pH is any $Hg(SR)_3^-$ formed when less than 2 equiv of peptide was present. Second, the initial increase in the formation of $Hg(SR)_3^-$ immediately after addition of 2 equiv was dependent on the pH. Third, the absorbance limit of the titration at high concentrations of peptide increases with pH. In the case of Tri L9C (with 5 μM $HgCl_2$ at pH 7) shown in Figure 4, the titration reached 95% of the maximum signal by 4 equiv. This result was observed for all pH values.

Global Analysis. All of the Hg titrations involving the addition of peptide into solutions of $HgCl_2$ were fit using the model:

$$L^- + H^+ \overset{\beta_{011}}{\rightleftharpoons} LH \tag{7}$$

$$3LH \overset{K_1}{\rightleftharpoons} (LH)_3 \tag{8}$$

$$Hg(II) + 2LH \overset{K_2}{\rightleftharpoons} Hg(II)(L)_2 + 2H^+ \tag{9}$$

$$Hg(II)(L)_2 + LH \overset{K_3}{\rightleftharpoons} Hg(II)(L)_2(LH) \tag{10}$$

$$Hg(II)(L)_2(LH) \overset{K_4}{\rightleftharpoons} Hg(II)(L_3)^- + H^+ \tag{11}$$

This representation must be expressed as formation constants (β_{mlh}) for input into the fitting software (Specfit, Spectrum Software Associates). Thus, K_2 can be expressed as $(\beta_{120})-(\beta_{001})^2/[(\beta_{011})^2(\beta_{100})]$, where β_{120} and β_{011} are formation constants for the two-stranded coiled coil with linear thiolato Hg(II) bound and the protonated peptide, respectively.

In a peptide unassociated with a coiled coil, we have assigned the pK_a of cysteine to be 8.5 [$(\log(\beta_{011}) = 8.5$], the pK_a of free cysteine in aqueous solutions. β_{033} was determined experimentally from guanidinium denaturations that determine $K_1 = \beta_{033}/\beta_{011}$. The value for β_{120} was taken to be 10^{60} on the basis of the formation constant of linear thiolato Hg(II) with simple ligands (*26*). The actual value for the peptide system is likely greater but this mechanism algorithm was unable to computationally accommodate greater values. We have found that β_{120} must be greater than 50 to obtain fits that reflect the data at less than 2 equiv of peptide added. The values for β_{130} and β_{131} are related by eq 5 (K_4) and were derived from a pH titration giving $\log(\beta_{131}) - \log(\beta_{130}) \approx 7.6$. This value was used to derive the initial estimates for the fits. The resulting values, taken from a series of fits for $\log(\beta_{131}) - \log(\beta_{130})$, were 7.3 $\pm$ 0.3 and 7.3 $\pm$ 0.5 for the titrations involving Baby L9C and Tri L9C, respectively; these values fell within error of the pK_a values of the mercurated three-stranded coiled coils, $HgL_2(LH)$, measured via direct titration.

This model took into account four thermodynamically important processes involved in trigonal thiolato Hg(II) three-stranded coiled coil (HgL_3^-) formation: the formation of the coiled coil in the absence of metal (β_{033}), the formation of $Hg(SR)_2$ (β_{120}), the formation of $HgL_2(LH)$ (β_{131}), and the formation of $Hg(SR)_3^-$ (β_{130}). There were three noteworthy omissions. No value was given for formation of a nonmetalated two-stranded coiled coil (β_{022}) because previous studies with the Tri series of peptides showed no significant concentration of two-stranded coiled coil in solution above pH 7 (*16*, *17*). Also, the deprotonation of a cysteine within the three-stranded coiled coil (β_{032}) was not accounted for because the expected pK_a of cysteine within the hydrophobic interior of three-stranded coiled coils would be significantly greater than the pK_a of cysteine in aqueous solution (pK_a =

8.5); therefore, it was assumed that the pK_a of the cysteine in the interior of the coiled coil is greater than 9.5. Last, formation of cystine dimer was not considered. Although formation of the cystine dimer is thermodynamically significant in aqueous solutions at pH >7, the dimerization requires the presence of an oxidant, usually O_2. The solutions were carefully purged with Ar prior to addition of peptide, and the solution was blanketed with N_2 throughout the titration. The concentration of the cystine dimer after the titrations was determined by analytical HPLC to be less than 5% of the total peptide concentration when pH ≤ 9.0. Under more basic conditions, the formation of the cystine dimer is significant enough to prevent adequate fitting of the data even with rigorous purging.

Size-Exclusion Chromatography. To verify the aggregation states of the peptides in solution, size-exclusion chromatography was performed using a Pharmacia Superdex 75 column using an eluant containing 150 mM sodium perchlorate buffered with 100 mM potassium phosphate at the desired pH. For each of the runs, arsenated peptide was used as a reference for the three-stranded coiled coil, and the cystine dimer was used as a reference for the two-stranded coiled coil.

The first experiment determined the aggregation of Baby L9C at pH 8.5 in the absence of metal. Baby L9C migrated with a larger retention volume than its corresponding cystine dimer and As(Baby L9C)$_3$. Furthermore, the peak corresponding to Baby L9C was much broader than either of the other two peptides. These results suggest that Baby L9C is a monomeric molten globule at pH 8.5 with multiple conformations.

The second experiment determined the aggregation state of Hg(Tri L9C)$_x^{+(2-x)}$ ($x = 2, 3$) at pH values ranging from 3 to 9. The results of this experiment are shown in Figure 5, where the relative retention time of the sample is given as a function of the retention times for the reference two- and three-stranded coiled coils:

$$\chi(\text{sample}) = [\text{RT(sample)} - \text{RT(dimer)}]/[\text{RT(trimer)} - \text{RT(dimer)}]$$

A plot of χ vs pH (Figure 5a) showed three general regions: at pH ≤4, the mercurated peptide migrated more closely to the dimer than the trimer. At pH values between 5 and 6, the mercurated peptide migrated between the dimer and the trimer. When pH ≥7, the migration of the mercurated peptide more closely resembled that of the trimer than the dimer. This experiment gives an apparent pK_a of the dimer to trimer transition in the 3:1 peptide:mercury mixture as 5.5 ± 1.

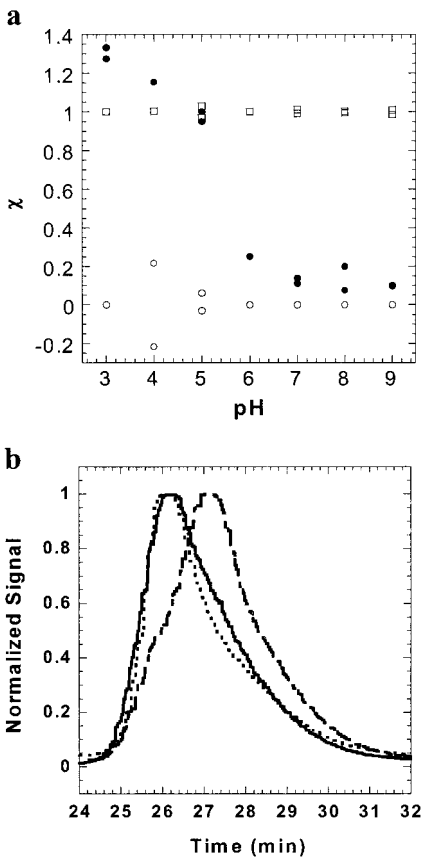

FIGURE 5: pH titration of a solution of 3:1 Tri L9C:$HgCl_2$ monitored using size-exclusion chromatography. The data are represented by χ, a function to describe the comparison between the retention time of the peptide aggregate with the retention times of a known dimer, (Tri L9C)$_2$, and trimer, As(Tri L9C)$_3$. (a) χ vs pH plot of Tri L9C + As(III) (trimer, ○), oxidized Tri L9C (dimer, □), and Tri L9C + $^1/_3HgCl_2$ (●). (b) Representative chromatograms for 3:1 Tri L9C:$HgCl_2$ (solid), As(Tri L9C)$_3$ (dotted), and 2:1 Tri L9C:$HgCl_2$ (dashed) at pH 7.0.

DISCUSSION

To understand further the factors that lead to stable metalloproteins, we have initiated a program to design small, untethered metallopeptide aggregates that provide variable coordination environements to metals. In particular, we have previously studied the binding of Hg to a family of peptides denoted the Tri family of peptides (*16*, *17*). This set of peptides is based on a 30 amino acid sequence, Ac-NH-G(LKALEEK)$_4$G-CONH$_2$, acetylated at the N-terminus and amidated at the C-terminus. The design includes a heptad repeat unit with hydrophobic residues in the a and d positions; this substitution pattern is typical of other α-helical peptides and α-helical portions of proteins found in nature. In the case of the Tri peptides, these hydrophobic residues drive the formation of a helical coiled coil into either a two- or three-stranded aggregate. In the absence of metals, the aggregation state is determined by the pH of the solution with three-stranded coiled coils dominating at high pH (pH >7) and two-stranded coiled coils dominating at low pH (pH <4).

Substitution of a leucine for a cysteine in either the a or d positions of the heptad resulted in a soft-metal binding site within the interior of the coiled coil. In a two-stranded coiled coil, this site consisted of two cysteine thiols and is capable of binding metal in a two-coordinate fashion. The site in the three-stranded coiled coil contained three thiols, making the coiled coil a trivalent ligand.

Hg(II) is a soft-metal ion that prefers to bind simple thiolates in aqueous solutions with a linear geometry at micromolar concentrations. Prior to investigations with the Tri series of peptides, the only aqueous system that was known to contain a trigonal thiolato coordination to a Hg(II) was the protein MerR, a mercury regulatory protein in bacteria. The peptides Tri L16C and Tri L9C provided a rigid trigonally symmetric framework prior to addition of metal

Scheme 1

SimAD: Simultaneous Aggregation-Deprotonation

$$HgCl_2 + 2\,HL \longrightarrow HgL_2 + 2\,HCl$$
$$HgL_2 + HL \rightleftharpoons HgL_3 + H^+$$

StepAD: Stepwise Aggregation-Deprotonation

$$HgCl_2 + 2\,HL \longrightarrow HgL_2 + 2\,HCl$$
$$HgL_2 + HL \rightleftharpoons HgL_2(LH)$$
$$HgL_2(LH) \rightleftharpoons HgL_3 + H^+$$

and were shown to bind the Hg(II) with trigonal coordination similarly to the MerR protein. Since this study, Li et al. have published the stabilization of trigonal thiolato coordination around Hg(II) using a different peptide, IZ-AC (*25*). IZ-AC was not a well-structured three-stranded coiled coil prior to addition of Hg(II); in fact, α-helix formation was induced upon addition of Hg(II). This result indicated that a rigid peptide backbone was not necessary for the formation of the alternate trigonal coordination around the Hg(II). The present work was directed toward understanding how the overall trigonal thiolato Hg(II) three-stranded coiled coil structure is stabilized.

An important observation from all of the Hg(II) binding peptide systems is that the aggregation state and the coordination geometry about the metal are dependent on the [peptide]/[Hg] ratio, denoted p/h. The three-stranded coiled coil with trigonal Hg(II) has never been observed at p/h ≤ 2 regardless of pH, concentration, or peptide sequence because the driving force for the formation of divalent Hg(II) with two thiolate ligands is large:

$$Hg^{2+} + RSH \rightleftharpoons Hg(SR)_2 + 2H^+ \qquad \Delta G = -78 \text{ kcal/mol}$$

The driving force for this reaction is greater than the free energy of peptide coiled-coil formation by at least 35 kcal/mol; coiled-coil formation free energy is about −40 kcal/mol for very strongly associated peptides. Thus, the preference for linear coordination around mercury would determine the structure of the Hg−peptide complex and result in a two-stranded coiled coil at p/h ≤ 2 for the systems described here. The problem then is a matter of describing the metallopeptide structure at higher concentrations of peptide.

For Tri L9C at p/h ≥ 2, the resulting aggregation state of the metal−peptide construct is pH dependent. At low pH (pH < 5), where the peptide prefers a two-stranded coiled-coil conformation, the metal−peptide complex remained a two-stranded coiled coil, $Hg(SR)_2$, at all concentrations of peptide and Hg(II) investigated. At higher pH, the situation was observed to be more complex in that there were two general models considered in this report for the binding of Hg(II) when p/h ≥ 2 at higher pH (Scheme 1).

The first model assumed that all mercury within a three-stranded coiled coil would be found in a trigonal thiolato coordination environment [$Hg(SR)_3^-$]. This model was termed the simultaneous aggregation-deprotonation (SimAD) model since formation of the three-stranded from the two-stranded coiled coil would require the concurrent deprotonation of the cysteine thiol to yield a trigonal thiolato Hg(II) complex. The second model allowed mercury to be found either in a trigonal coordination environment [$Hg(SR)_3^-$] or in a linear coordination environment within the three-stranded coiled coil, $Hg(SR)_2(RSH)$, the third cysteine having been protonated and either loosely associated with Hg(II) or completely unbound. This model is referred to as the stepwise aggregation-deprotonation (StepAD) model because formation of the trigonal thiolato mercury requires two separate steps: the aggregation of the peptides and the deprotonation of the thiol. It is important to note that these two mechanisms converge under strongly basic conditions (pH $\gg$ pK_a of the third thiol within the mercurated three-stranded coiled coil).

Looking at Scheme 1, there are some experimental observations that can be made to differentiate between the models for the Tri series of peptides. In the SimAD model, the apparent pK_a of the transition between the linear thiolato Hg(II) and the trigonal thiolato Hg(II) may be influenced by the Gibb's free energy of coiled-coil association. This would not be the case in the StepAD model where coiled-coil formation occurs in the step prior to deprotonation. The similar pK_a values for this transition, Tri L9C (p$K_a = 7.6 \pm 0.2$) and Baby L9C (p$K_a = 7.7 \pm 0.2$), would seem to support the StepAD model (Figure 2). However, in the SimAD model formation of the trigonal thiolato mercury requires both construction of a three-stranded coiled coil with Hg(II) and destruction of the nonmetalated three-stranded coiled coil. Thus, no change in the apparent pK_a would be observed if the energy of the two processes were equal and opposite or if they differed by a constant energy in both the Tri L9C and Baby L9C systems. The probability of this coincidence occurring is high because the peptide structure in both the metalated and unmetalated peptide coiled coils is likely similar. Therefore, this result was at best circumstantial evidence supporting the StepAD model.

Also in the SimAD model, the addition of excess peptide at pH values less than or equal to the apparent pK_a of the trigonal thiolato Hg formation would drive the reaction toward formation of trigonal coordination; that is, the apparent pK_a would be dependent on [peptide]. In the StepAD model, only formation of the linear thiolato Hg(II) three-stranded coiled coil would be influenced by addition of excess peptide; formation of trigonal thiolato Hg(II) would only be dependent on pH. Thus, the apparent pK_a would not be dependent on [peptide] in the StepAD model. Figure 4 shows a titration of Tri L9C into Hg(II) at pH 7.0 with fits for both the SimAD and StepAD mechanisms included. After 4 equiv of peptide had been added, there was no significant increase in UV signal for the data, indicating no increase in the amount of trigonally ligated Hg(II) present in solution. The StepAD model fit these data well, whereas the SimAD model predicted an increasing amount of HgL_3^- as the concentration of the peptide was increased. In addition, as the concentration of peptide increased past 2 equiv, the slope of the data more closely resembled that of the StepAD model.

The major difference between the SimAD and the StepAD models was that the StepAD model accounted for the presence of a three-stranded coiled coil containing linearly coordinated Hg(II) whereas the SimAD model did not. For Tri L9C, the SimAD model predicts that the apparent pK_a of the two- to three-stranded coiled-coil transition in the presence of $^1/_3$ equiv of Hg(II) should correspond to that for the linear to trigonal thiolato Hg transition (p$K_a = 7.6 \pm 0.2$). The StepAD model predicted that the pK_a of the transition between coiled-coil aggregation states in the

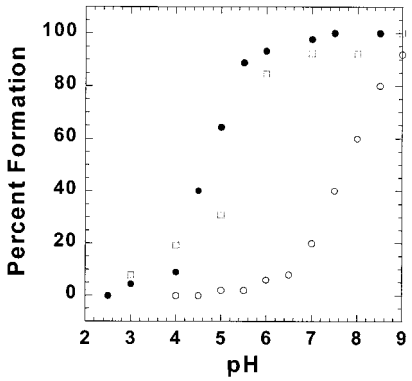

FIGURE 6: Percent formation vs pH plot for the formation of a three-stranded coiled coil in the absence of Hg(II) from guanidinium denaturation studies (●; *16*), the formation of a three-stranded coiled coil in the presence of Hg(II) from size-exclusion chromatography (□), and the formation of trigonal thiolato Hg(II) within the interior of a three-stranded coiled coil (○).

Table 3: Formation Constants for Species Involved in the Formation of the Trigonal Thiolato Hg(II) Encapsulated in a Three-Stranded Coiled Coil for Baby L9C and Tri L9C[a]

	Baby L9C	Tri L9C
formation constants		
$\log[\beta_{011}\ (M^{-1})]$	8.5[b]	8.5[b]
$\log[\beta_{033}\ (M^{-5})]$	32.5[c]	38.9[c]
$\log[\beta_{120}\ (M^{-2})]$	60.0[d]	60.0[d]
$\log[\beta_{130}\ (M^{-3})]$	65.5 (2)	68.4 (5)
$\log[\beta_{131}\ (M^{-4})]$	72.8 (3)	75.7 (5)
other equilibria (log *K*)		
$\log K_3$	4.3 (3)	7.1 (5)
$\log K_4$	−7.3 (3)[e]	−7.3 (4)[e]
$LH \rightleftharpoons {}^1/_3(LH)_3$ ($^1/_3K_a$)	2.6 (3)	4.4 (3)

[a] Values in parentheses indicate the certainty of the last significant digit. These errors are from a series of fits using β_{033} as an absolute value. [b] pK_a of free cysteine in solution. [c] Derived from values in Table 2 obtained by guanidinium denaturations ($\beta_{033} = 3\beta_{011} - \log K_d$). [d] Taken from the value for simple thiolate ligands (*26*). [e] The pK_a of the cysteine thiol within a mercurated three-stranded coiled coil derived from fits to the Hg titration data is within error of that derived from pH titrations of the mercurated three-stranded coiled coil, which are 7.6 (2) and 7.7 (2) for Tri L9C and Baby L9C, respectively.

presence of $^1/_3$ equiv of Hg(II) may correspond to the apparent pK_a of the same transition in the absence of Hg(II) (pK_a ∼ 5.5). Size-exclusion chromatography (Figure 5) indicated that, in a solution of Tri L9C with p/h = 3, the pK_a of the two- to three-stranded coiled coil transition occurred between pH 5 and pH 6. This transition was well below that predicted in the SimAD model (∼7.5). This result, in conjunction with the observation that the linear to trigonal thiolato Hg(II) transition occurred at pH 7.6, indicated the presence of a significant amount of three-stranded coiled coil containing linear mercury between pH 6 and pH 8 (Figure 6). This observation invalidated the SimAD model and again supported the StepAD model.

Given these three results, the StepAD model was used to fit titration data and obtain quantitative information about the mercurated peptide systems (Table 3). The results supported the formation of the mercurated two-stranded coiled coil (HgL_2) as the most thermodynamically favorable reaction in the solution. Furthermore, Hg(II) binding drives folding of the three-stranded coiled coil by forcing the peptide to adopt two-stranded coiled-coil structure. At high pH, the driving force for the addition of the third strand into the mercurated coiled coil ($\log K_3$) was greater than one-third the formation constant of the unmetalated three-stranded coiled coil ($\log K_a$). Hg(II) binding may have decreased the entropic tendency for the three-stranded coiled coil to dissociate by effectively clamping two helices together. The resulting structure was a mercurated three-stranded coiled coil. Mercury also aids in the formation of a trigonal ligation geometry by lowering the pK_a of the third cysteine thiol in the hydrophobic core of the coiled coil from a value of >8.5 to 7.6 ± 0.2. We cannot discern whether this pK_a drop is due simply to the proximity of the Hg to the third cysteine thiol or whether the sulfur is weakly bound to the Hg(II) as a thiol group. Whatever the mechanism, the pK_a of cysteine was shifted into a range where it could be deprotonated, allowing the formation of the trigonal thiolato Hg(II).

One may next consider the necessity of having a preorganized site in a structured peptide for efficient metal recognition. In the absence of metal, Tri L9C formed structured two-stranded coiled coils or three-stranded α-helical coiled coils, depending on pH. However, an important prediction of the StepAD model is that the peptide does not need to be structured prior to the addition of the Hg(II). Since the driving force of forming the linear Hg(II) thiolate two-stranded coiled coil is large, the ultimate factor in determining the final aggregation state of the peptide was the driving force between the mercurated two-stranded coiled coil and the final structure of the peptide. This explanation underscores why a rigid, preorganized structure is not necessarily required for the stabilization of an alternate coordination environment around Hg(II), a hypothesis that can be tested using Baby L9C, which is destabilized from Tri L9C by removal of seven amino acids. The deletion of a heptad removed two turns of the α-helix per peptide, resulting in the elimination of six leucines that drive the formation of the three-stranded coiled coil. The driving force for the formation of this coiled coil was then ∼8 kcal/mol less than that for Tri L9C. As a result, Baby L9C was unstructured at micromolar concentrations. Addition of $HgCl_2$ to a 10 μM solution of Baby L9C led to significant enhancement of the CD signal at 222 nm up to p/h = 2 (Figure 7). The strong enthalpic driving force to form $Hg(II)L_2$ overwhelmed the entropic barrier to coiled-coil formation, and the α-helix was stabilized by the complexation of mercury. However, the coordination preference of Hg(II) is linear, not trigonal. If metal coordination preference was the sole contributor to overall structure, the final structure would be a two-stranded coiled coil with bound linear Hg(II).

Although the coiled coil was assembled by Hg(II), the peptide aggregation state preference dictated the final structure. The trimeric form of the peptide was more stable than the dimer at pH conditions more basic than 5.5. As a result, the Hg(II) was encapsulated within a three-stranded coiled coil. Formation of the three-stranded coiled coil brought the third cysteine thiolate to the proximity of the Hg(II), effectively lowering the pK_a to 7.7 ± 0.2. We concluded that both of the geometrical preferences of the metal and the peptide were contributing to the final structure: the peptide will not fold without the metal, but the final fold is dictated by the peptide, not the metal. Under appropriate conditions, this aggregation preference can be used to enforce an alternate metal coordination geometry. Thus, not only does the Hg(II) stabilize the formation of the

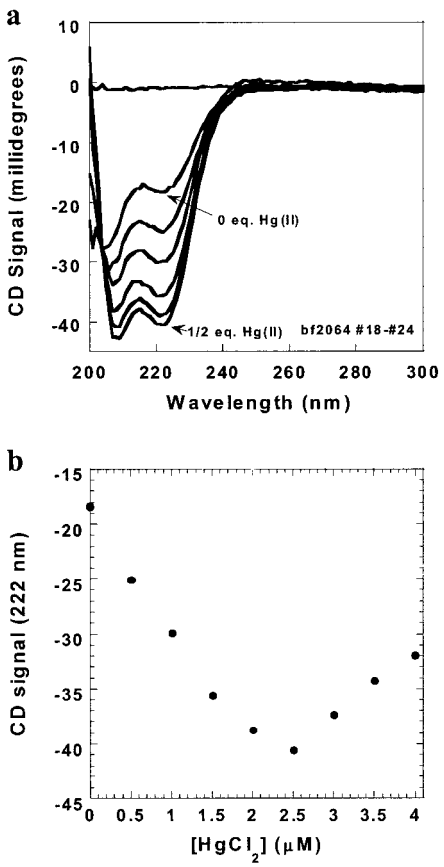

FIGURE 7: (a) Titration of $HgCl_2$ into a solution of 5 μM Baby L9C in 50 mM potassium phosphate buffer, pH 8.5, monitored by circular dichroism spectroscopy and (b) the trace at 222 nm (the maximum signal for an α-helix).

coiled coil but the structure of the peptide stabilizes the formation of a trigonal thiolato Hg(II).

This thermodynamic model for complexation can be used to propose a kinetic mechanism for cooperative folding of a three-stranded coiled coil around trigonal thiolato Hg(II) by an unstructured peptide, like Baby L9C (Scheme 2). The initial step in this reaction is the formation of the linearly coordinated Hg(II) within a two-stranded coiled coil (HgL_2), a structure governed by the desired metal coordination geometry. This step is proposed to be relatively fast because of the large driving force. The second step of the reaction is the addition of a third strand to form the three-stranded coiled coil encapsulating Hg(II) with linear coordination, a structure stabilized by the structural preference of the peptide. Since the driving force for this step is significantly smaller than the initial binding of Hg(II), this step is proposed to be slower than the initial step. Last, the third cysteine thiol is deprotonated, and the trigonal thiolato Hg(II) is formed. This step may be fast, depending on the exposure of the thiol to the surrounding solution.

If the deprotonation is fast relative to three-stranded coiled-coil formation, this proposed mechanism would display biphasic binding kinetics, a fast step followed by a slower step. This type of biphasic folding kinetics from unstructured polypeptide chains to folded protein structure has been observed in the study of natural enzyme systems that involve inorganic cofactors. Perhaps the most well documented example is that for the folding of cytochrome *c* (*22*, *32*−*34*). Cytochrome *c* contains a heme prosthetic group that is covalently linked to the polypeptide chain by two cysteine sulfur linkages; the iron is axially ligated by a histidine and a methionine in its folded state. When the Fe(III) form of the protein is kept in a solution of concentrated denaturant, the heme−methionine interaction is broken and replaced by a histidine bond, providing bis-histidine ligation to the heme. A histidine has been demonstrated to have stronger interactions with an Fe(III) heme−histidine peptide complex than a methionine (*35*). If the denaturant is quickly diluted by the addition of excess buffer, the kinetics of the folding can be observed. The kinetics are biphasic. The first step, termed the nascent stage of folding, is responsible for the initial collapse of the polypeptide chain into a compact structure while maintaining the bis-histidine ligation of the Fe(III) heme. The second slower step, termed the ligand exchange phase, is responsible for determining the final structure of the protein. This second step involves axial ligand exchange that selects the most thermodynamically favored cofactor−protein conformation and is directed by an interplay between the desired protein structure and the metal−ligand interactions. In cytochrome *c*, the final structure contains a heme complex axially ligated by a histidine and a methionine.

Our proposed folding mechanism of $Hg(II)(Baby\ L9C)_3$ formation can be compared to the folding of cytochrome *c* where the driving force and initial collapse of the structure involve a strong ligation around the metal center. In ferricytochrome *c* the collapsed protein contains a pair of nitrogen donor ligands for the axial coordination to the heme, whereas the case of Hg(II) peptide contains a linear thiolato Hg(II). The second stage of both reactions involves the stabilization of a separate ligation environment around the metal by the polypeptide fold. In cytochrome *c*, the protein fold directs a methionine−histidine ligation for the heme via a ligand exchange/selection process. In the case $Hg(II)(Baby\ L9C)_3$, the desired conformation of the peptide, a three-stranded coiled coil, directs trigonal ligation about the Hg(II),

Scheme 2

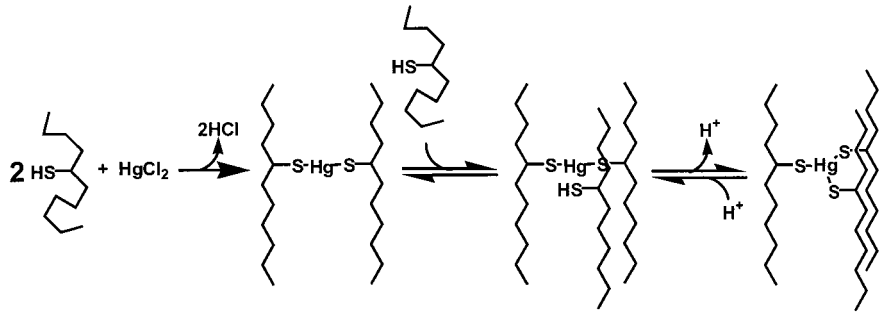

a geometry that is not normally favored at micromolar concentrations. In cytochrome *c*, this second step involves an array of misligated and misfolded states that complicates the folding process (*34*). Our example provides a simplified model that can be used to study cooperative metalloprotein folding.

CONCLUSIONS

A detailed thermodynamic analysis of the folding of a three-stranded coiled coil around Hg(II) has been presented. This analysis has resulted in a unified model that explains how systems such as Baby L9C and IZ-AC that do not form well-defined structures prior to binding Hg(II) and systems such as Tri L9C that form well-defined three-stranded coiled coils in the absence of Hg(II) can enforce a trigonal thiolato Hg(II) environment under conditions where linear coordination with simple thiolate ligands is preferred. The StepAD model supports the formation of a linear dithiolato Hg(II) encapsulated within a three-stranded coiled coil at a binding site contianing three cysteine thiols. This model also suggests that stabilization of the trigonal thiolato Hg(II) at more acidic pH values than previously observed cannot be achieved simply by increasing the driving force of coiled-coil formation because the formation of the trigonal thiolato Hg(II) is a result of a deprotonation of a cysteine thiol within the three-stranded coiled coil and not a direct result of coiled-coil formation. Last, the complexation of Hg(II) by Baby L9C is consistent with a biphasic kinetic mechanism for peptide folding around Hg(II) that may be analogous to the intermediate folding states for metalloproteins in vitro and in vivo.

ACKNOWLEDGMENT

The authors thank Emmanouil Matzapetakis for helpful discussions and Tsu-Chien Weng and the laboratory of Prof. James E. Penner-Hahn for help in writing the script to fit the guanidinium denaturations.

REFERENCES

1. DeGrado, W. F., Summa, C. M., Pavone, V., Nastri, F., and Lombardi, A. (1999) *Annu. Rev. Biochem. 68*, 779−819.
2. Mant, C., Zhou, N. E., and Hodges, R. S. (1993) *Amphipathic Helix*, pp 39−64, CRC Press, Boca Raton, FL.
3. Hill, R. B., Raleigh, D. P., Lombardi, A., and DeGrado, W. F. (2000) *Acc. Chem. Res 33*, 745−754.
4. Hodges, R. S. (1996) *Biochem. Cell Biol. 74*, 133−154.
5. Ghadiri, M. R., Soares, C., and Choi, C. (1992) *J. Am. Chem. Soc. 114*, 825−831.
6. Hellinga, H. W. (1998) *Folding Des. 3*, R1−R8.
7. Xing, G., and DeRose, V. J. (2001) *Curr. Opin. Chem. Biol. 5*, 196−200.
8. Berg, J. M., and Godwin, H. A. (1997) *Annu. Rev. Biophys. Biomol. Structure 26*, 357−371.
9. Randall, D. W., Gamelin, D. R., LaCroix, L. B., and Solomon, E. I. (2000) *J. Biol. Inorg. Chem 5*, 16−19.
10. Case, M. A., Ghadiri, M. R., Mutz, M. W., and McLendon, G. L. (1998) *Chirality 10*, 35−40.
11. Ghadiri, M. R., and Case, M. A. (1993) *Angew. Chem., Int. Ed. Engl. 32*, 1594−1597.
12. Mutz, M. W., Case, M. A., Wishart, J. F., Ghadiri, M. R., and McLendon, G. L. (1999) *J. Am. Chem. Soc. 121*, 858−859.
13. Kozlov, G. V., and Ogawa, M. Y. (1997) *J. Am. Chem. Soc. 119*, 8377−8378.
14. Kornilova, A. Y., Wishart, J. F., Xiao, W., Lasey, R. C., Federova, A., Shin, Y.-K., and Ogawa, M. Y. (2000) *J. Am. Chem. Soc. 122*, 7999−8006.
15. Suzuki, K., Hiroaki, H., Kohda, D., Nakamura, H., and Tanaka, T. (1998) *J. Am. Chem. Soc. 120*, 13008−13015.
16. Dieckmann, G. R., McRorie, D. K., Lear, J. D., Sharp, K. A., DeGrado, W. F., and Pecoraro, V. L. (1998) *J. Mol. Biol. 280*, 897−912.
17. Dieckmann, G. R., McRorie, D. K., Tierney, D. L., Utschig, L. M., Singer, C. P., O'Halloran, T. V., Penner-Hahn, J. E., DeGrado, W. F., and Pecoraro, V. L. (1997) *J. Am. Chem. Soc. 119*, 6195−6196.
18. Hellinga, H. W. (1998) *J. Am. Chem. Soc. 120*, 10055−10066.
19. Pinto, A. L., Hellinga, H. W., and Caradonna, J. P. (1997) *Proc. Natl. Acad. Sci. U.S.A. 94*, 5562−5567.
20. Benson, D. E., Wisz, M. S., and Hellinga, H. W. (2000) *Proc. Natl. Acad. Sci. U.S.A. 97*, 6292−6297.
21. Marvin, J. S., and Hellinga, H. W. (2001) *Proc. Natl. Acad. Sci. U.S.A. 98*, 4955−4960.
22. Englander, S. W., Sosnick, T. R., Mayne, L. C., Shtilerman, M., Qi, P. X., and Bai, Y. (1998) *Acc. Chem. Res. 31*, 737−744.
23. Gibney, B. R., Rabanal, F., Skalicky, J. J., Wand, A. J., and Dutton, P. L. (1999) *J. Am. Chem. Soc. 121*, 4952−4960.
24. Gibney, B. R., Mulholland, S. E., Rabanal, F., and Dutton, P. L. (1996) *Proc. Natl. Acad. Sci. U.S.A. 93*, 15041−15046.
25. Li, X., Suzuki, K., Kanaori, K., Tajima, K., Kashiwada, A., Hiroaki, H., Kohda, D., and Tanaka, T. (2000) *Protein Sci. 9*, 1327−1333.
26. Wright, J. G., Natan, M. J., MacDonnell, F. M., Ralston, D. M., and O'Halloran, T. V. (1990) *Prog. Inorg. Chem. 38*, 323−412.
27. Su, J. Y., Hodges, R. S., and Kay, C. M. (1994) *Biochemistry 33*, 15501−15510.
28. Pace, C. N., and Scholtz, J. M. (1997) in *Protein Structure: A Practical Approach* (Creighton, T. E., Ed.) pp 299−321, Oxford University Press, Oxford.
29. Boice, J. A., Dieckmann, G. R., DeGrado, W. F., and Fairman, R. (1996) *Biochemistry 35*, 14480−14485.
30. Fairman, R., Chao, H.-G., Mueller, L., Lavoie, T. B., Shen, L., Novotny, J., and Matsueda, G. R. (1995) *Protein Sci. 4*, 1457−1469.
31. Farrer, B., McClure, C., Penner-Hahn, J. E., and Pecoraro, V. L. (2000) *Inorg. Chem. 39*, 5422−5423.
32. Shastry, M. C. R., Sauder, J. M., and Roder, H. (1998) *Acc. Chem. Res. 31*, 717−725.
33. Yeh S.-R., Han S., and Rousseau D. L. (1998) *Acc. Chem. Res. 37*, 727−736.
34. Tezcan, F. A., Winkler, J. R., and Gray, H. B. (1999) *J. Am. Chem. Soc. 121*, 11918−11919.
35. Tezcan, F. A., Winkler, J. R., and Gray, H. B. (1998) *J. Am. Chem. Soc. 120*, 13383−13388.

BI015649A